Reconstruction of implanted marker trajectories from cone-beam CT projection images using interdimensional correlation modeling

Hyekyun Chung[1, 2], Per Rugaard Poulsen[3], Paul J. Keall[4], Seungryong Cho[1] and Byungchul Cho[2]

[1] *Department of Nuclear and Quantum Engineering, Korea Advanced Institute of Science and Technology, Daejeon, Korea*

[2] *Department of Radiation Oncology, Asan Medical Center, University of Ulsan College of Medicine, Seoul, Korea*

[3] *Department of Oncology, Aarhus University Hospital, Aarhus, Denmark*

[4] *Radiation Physics Laboratory, Sydney Medical School, University of Sydney, Sydney, Australia*

***Corresponding Author Contact Information:**

Byungchul Cho, Ph.D.

Department of Radiation Oncology

Asan Medical Center, University of Ulsan College of Medicine

86 Asanbyeongwon-gil, Songpa-gu, Seoul 138-736, Korea

Tel: +82 2 3010 4437, C.P.: +82 3203 4437

E-mail: cho.byungchul@gmail.com, bcho@amc.seoul.kr

Running Head: 3D trajectory reconstruction from CBCT projection images

Acknowledgment: This work was supported by the National Research Foundation of Korea (NRF) grant funded by the Korea government (MSIP) (No. 2015038710).

Submitted to: Medical Physics as a research paper.

ABSTRACT

Purpose: Cone-beam CT (CBCT) is a widely used imaging modality for image-guided radiotherapy (IGRT). Most vendors provide CBCT systems that are mounted on a linac gantry. Thus, CBCT can be used to estimate the actual 3-dimensional (3D) position of moving respiratory targets in the thoracic/abdominal region using 2D projection images. We have developed a method for estimating the 3D trajectory of respiratory-induced target motion from CBCT projection images using interdimensional correlation modeling.

Methods: Because the superior–inferior (SI) motion of a target can easily be analyzed on projection images of a gantry-mounted CBCT system, we investigated the interdimensional correlation of the SI motion with left–right (LR) and anterior–posterior (AP) movement while the gantry is rotating. A simple linear model and a state-augmented model were implemented and applied to the interdimensional correlation analysis, and their performance was compared. The parameters of the interdimensional correlation models were determined by least-square estimation of the 2D error between the actual and estimated projected target position. The method was validated using 160 3D tumor trajectories from 46 thoracic/abdominal cancer patients obtained during CyberKnife treatment. Our simulations assumed two application scenarios: (1) retrospective estimation for the purpose of moving tumor setup used just after volumetric matching with CBCT; and (2) on-the-fly estimation for the purpose of real-time target position estimation during gating or tracking delivery, either for full-rotation volumetric-modulated arc therapy (VMAT) in 60 s or a stationary six-field intensity-modulated radiation therapy (IMRT) with a beam delivery time of 20 s.

Results: For the retrospective CBCT simulations, the mean 3D root-mean-square error (RMSE) for all 4893 trajectory segments was 0.41 mm (simple linear model) and 0.35 mm (state-augmented model). In the on-the-fly simulations, prior projections over more than 60° appear to be necessary for reliable estimations. The mean 3D RMSE during beam delivery after the simple linear model had established with a prior 90° projection data was 0.42 mm for VMAT and 0.45 mm for IMRT.

Conclusions: The proposed method does not require any internal/external correlation or statistical modeling to estimate the target trajectory, and can be used for both retrospective image-guided radiotherapy with CBCT projection images and real-time target position monitoring for respiratory gating or tracking.

Keywords: Image-guided radiation therapy, Cone-beam CT, respiratory motion, Real time tumor tracking

I. INTRODUCTION

In radiotherapy, accurate dose delivery is essential to sufficiently treat tumors and prevent side effects in healthy surrounding tissues that are exposed to radiation. However, tumor motion increases treatment uncertainty, and can lead to an increased radiation dose to normal tissues.[1] Tumors in the thorax and abdomen are subject to such motion as a result of breathing and other intrafractional organ movements.

Gating and tumor-tracking are useful methods for overcoming motion-related problems. These methods are widely applied in current image-guided radiotherapy (IGRT) techniques to ensure accurate dose delivery to the target and reduce exposure to healthy tissues.[2, 3]

Real-time three-dimensional (3D) tumor position monitoring is a key technique for managing respiratory tumor motion in such gating and tracking approaches.[4] Stereoscopic X-ray imaging systems such as CyberKnife (Accuray Inc., Sunnyvale, CA), Novalis Tx (BrainLab AG, Munich, Germany and Varian Medical Systems, Palo Alto, CA), and Mitsubishi/Hokkaido RTRT systems can locate tumors in 3D.[5, 6] Stereoscopic imaging, which uses synchronous or alternate dual radiographic imagers, can theoretically locate 3D target positions via triangulation. However, stereoscopic imaging systems are not widely used because of their high cost, complexity of installation, and relatively small field of view.[6]

Instead, monoscopic (i.e., single) kV imagers are commonly used in modern radiotherapy machines such as on-board imaging systems. Several methods for estimating the 3D target position using monoscopic images have recently been published.[7-11] However, these methods are either somewhat inaccurate or do not provide results in real time. To overcome the drawbacks of these target estimation methods, probability-based methods that use single imagers have been developed for target localization.[6,12] Poulsen *et al.*[12] assumed 3D Gaussian distributions to determine the tumor position on projected images, allowing the tumor trajectory to be estimated accordingly, whereas Li *et al.*[6] used a Bayesian approach to find a proper probability density function that accounted for real respiratory motions, which may be asymmetrical, multimodal, or hysteric. Additionally, Becker *et al.*[13] and Park *et al.*[14] estimated 3D target trajectories geometrically based on the assumption that the 3D target positions are confined within some combination of respiratory, oscillatory, and fixed trajectories.

To a certain extent, respiratory motions are correlated either inter-dimensionally (e.g., correlation between superior–inferior (SI) and anterior–posterior (AP) motion) or with an external surrogate motion through the biomechanical characteristics of respiration. Thus, correlation models could effectively estimate the tumor positions from 2D projection images.

In this work, we propose an interdimensional correlation model for estimating the 3D target trajectory of respiratory-induced motion using cone-beam CT (CBCT) projection images. We determine the projected target positions using real patient data that contain implanted markers. The 3D marker positions are reconstructed from the projected positions using least-squares estimation (LSE) to determine the parameters for the interdimensional correlation model.

To evaluate the estimation performance of the proposed method, a series of simulations were performed under two application scenarios. First, for the purpose of a moving tumor setup used just after volumetric matching with CBCT, an interdimensional correlation model was built using full-rotation projection data from a CBCT scan. This model was then retrospectively applied to the projection data to estimate the 3D position of the tumor. Second, for the purpose of real-time target position monitoring during respiratory gating or tracking delivery for either volumetric-modulated arc therapy (VMAT) or intensity-modulated radiation therapy (IMRT), an interdimensional correlation model was initialized using a limited range of angular projection data. This model was updated on-the-fly each time new projection data were added and used to estimate the 3D position of the new projection data.

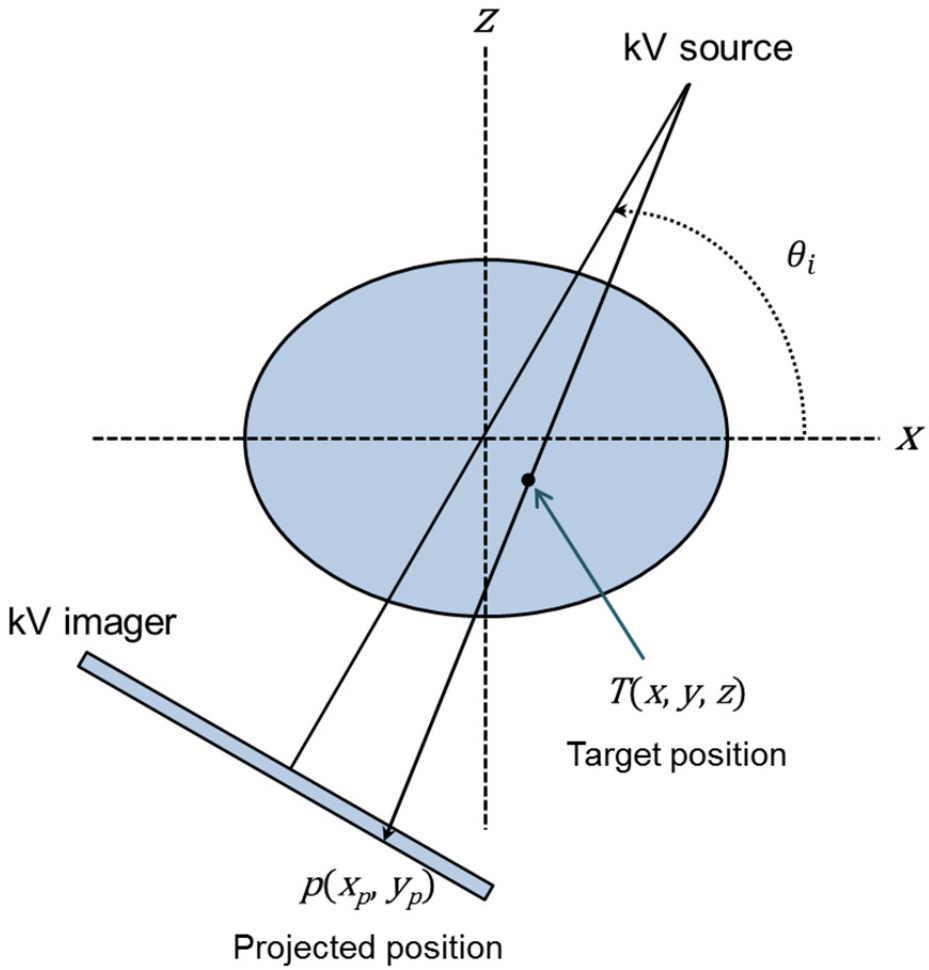

Figure 1. Schematic of a CBCT projection imaging system that uses a single kV X-ray imager.

105

II. METHODS AND MATERIALS

2.1. Interdimensional correlation model (IDCM)

As shown in Fig. 1, a conventional geometric configuration of the OBI CBCT imaging system was used.[15] The target positions are represented by x, y, and z along the left–right (LR), superior-inferior (SI), and anterior-posterior (AP) directions, respectively. The projected position $\mathbf{p}(x_p, y_p)$ on the image plane of a target position $\mathbf{T}(x, y, z)$ can be formulated by

$$\begin{pmatrix} x_p \\ y_p \end{pmatrix}^{\theta_i} = \frac{1}{f(\theta_i)} \begin{pmatrix} x \cdot \sin\theta_i - z \cdot \cos\theta_i \\ y \end{pmatrix}. \\ = P(\theta_i)(x, y, z) \tag{1}$$

In Eq. (1), the perspective term $f(\theta_i)$ is defined by:

$$f(\theta_i) = \frac{SAD - [x \cdot \cos\theta_i + z \cdot \sin\theta_i]}{SID}, \tag{2}$$

where SAD and SID are the source-to-axis distance and the source-to-imager distance, respectively. θ_i represents the gantry angle of the i^{th} view position. $\mathbf{P}(\theta_i)$ is a projection operator that maps the 3D target position $\mathbf{T}(x, y, z)$ to the projected position $\mathbf{p}(x_p, y_p)$. In this study, SAD = 100 cm and SID = 150 cm. Equations (1) and (2) were used to simulate the CBCT data acquisition of a clinical 3D tumor trajectory. In addition, the relationship between y and y_p ($y = f(\theta_i) \times y_p$) from Eq. (1) was used to determine y from the projected position.

To estimate the 3D trajectory of respiration-induced motion using CBCT projection images, each direction of the respiration-induced target motion was correlated interdimensionally. In particular, SI motion is always resolved on projection images, because it runs along the axis of rotation of the CBCT acquisition. Therefore, the SI motion was linked to other dimensions as:

$$\begin{pmatrix} \hat{x}(t) \\ \hat{z}(t) \end{pmatrix} = \begin{pmatrix} a_x \\ a_z \end{pmatrix} \hat{y}(t) + \begin{pmatrix} b_x \\ b_z \end{pmatrix}, \tag{3}$$

where $\mathbf{a}=(a_x, a_z)^T$ and $\mathbf{b}=(b_x, b_z)^T$ are the model parameters of this interdimensional correlation, and $\hat{x}$, $\hat{y}$, and $\hat{z}$ are the estimated target positions as a function of time.

Equation (3) represents a simple linear correlation model. To better model the correlation for hysteric motions, a state-augmented model has been proposed.[16] We incorporated this state-augmented model to address the motion correlation in CBCT projection images. The state-augmented model ($\mathbf{T}(t) = \mathbf{a}y(t) + \mathbf{b}y(t - \tau) + \mathbf{c}$) can be written in our interdimensional correlation model as:

$$\begin{pmatrix} \hat{x}(t) \\ \hat{z}(t) \end{pmatrix} = \begin{pmatrix} a_x \\ a_z \end{pmatrix} \hat{y}(t) + \begin{pmatrix} b_x \\ b_z \end{pmatrix} \hat{y}(t-\tau) + \begin{pmatrix} c_x \\ c_z \end{pmatrix}. \tag{4}$$

The time lag τ was set to 0.6 s, as will be discussed in Section 4. Note that the projection data $y(t–\tau)$ required for the 3D position estimation from the current projection data $y(t)$ are previous data acquired $\tau = 0.6$ s before. Thus, this computation does not cause any time delay for real-time applications. In this study, we applied both the simple linear form and the state-augmented form to the interdimensional correlation analysis of clinical data.

For m given projections $\mathbf{p}(x_p(\theta_i), y_p(\theta_i); \{t_1:t_m\})$ that are sequentially measured at various projection angles θ_i at time points t_i, LSE was performed to determine the correlation model parameters:

$$(\hat{a}, \hat{b}) = \arg\min_{i=1}^{m} \left\| p(x_p, y_p; t_i) - P(\theta_i)(\hat{x}, \hat{y}, \hat{z}) \right\|^2. \tag{5}$$

$\mathbf{P}(\theta_i)$ represents the projection operation, including rotation transforms, in Eqs. (1) and (2). We determined the model parameters (**a, b**) in Eq. (3) and (**a, b, c**) in Eq. (4) by solving the optimization problem in Eq. (5). The model parameters that minimize the square error $\| \mathbf{p}(x_p, y_p; t_i) - \mathbf{P}(\theta_i)(\hat{x}, \hat{y}, \hat{z}) \|^2$ are selected as solutions. The method of least squares was employed to optimize the model parameters.

The unknown model parameters can be exactly calculated from $\mathbf{p}(x_p(\theta_i), y_p(\theta_i))$, which are already known, and $\mathbf{P}(\theta_i)$ and y, which can be derived from Eq. (1). However, the LSE of Eq. (5) cannot be obtained directly, because the perspective term $f(\theta_i)$ is not explicitly included. Accurate values of x and z are needed to calculate $f(\theta_i)$ accurately. However, x and z are unknown values that depend on the model parameters. Therefore, we employed an iterative approach to solve this problem. We initially approximated $f(\theta_i)$ as:

$$f(\theta_i) = \frac{SAD - [x \cdot \cos\theta_i + z \cdot \sin\theta_i]}{SID} \approx \frac{SAD}{SID}. \quad (6)$$

This approximation is reasonable, as the coordinates of the target position x and z are usually much smaller than the SAD.

Using this approximation, the LSE determines the model parameters a, b, and c. After the first optimization of the model parameters, the x and z values are calculated again using Eqs. (3) and (4). Subsequently, $f(\theta_i)$ is updated using the new values of x and z, and on the process is repeated. This procedure was iterated five times, after which $f(\theta_i)$ had converged to within some preset tolerance. The overall process is schematically summarized in Fig. 2.

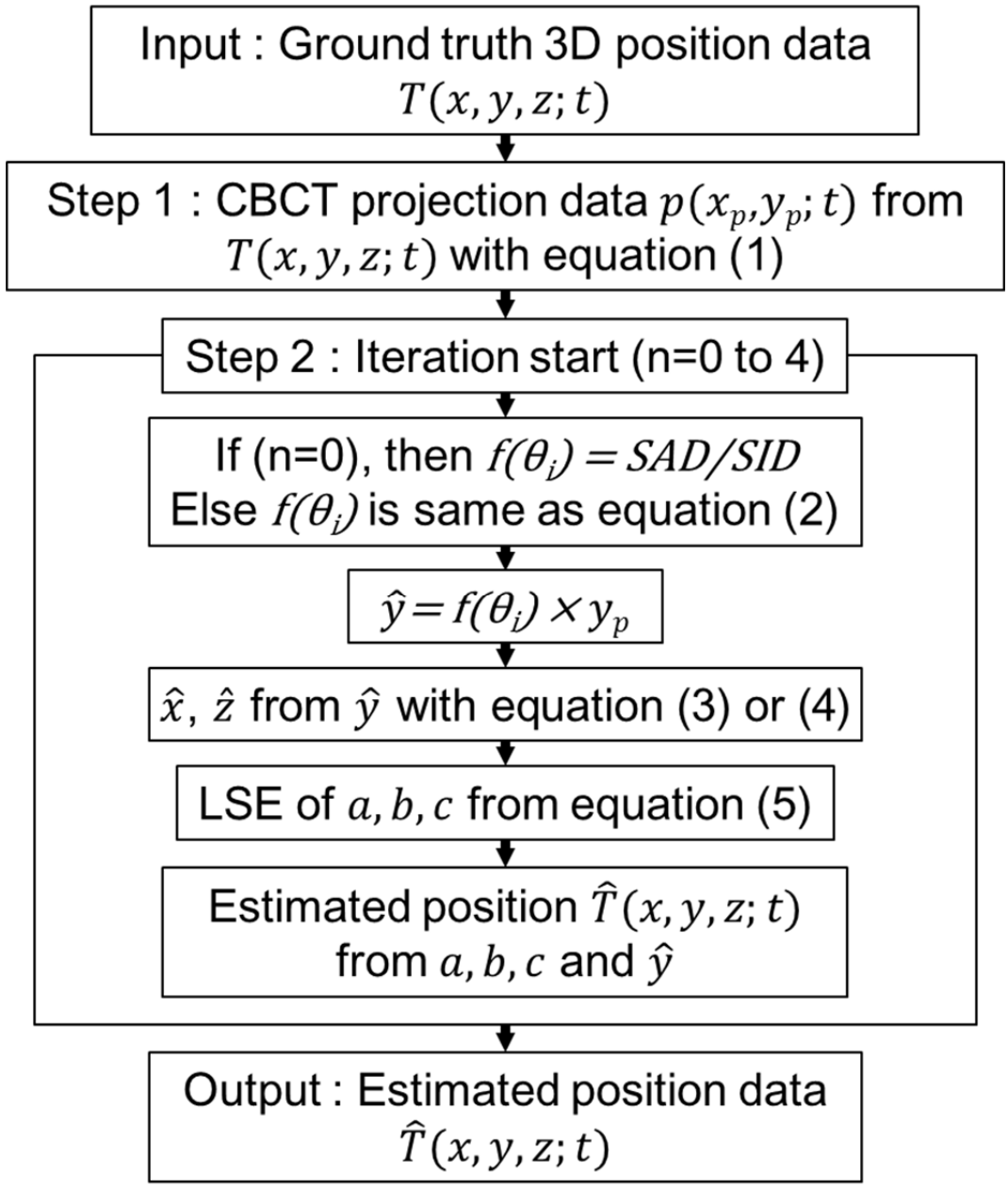

Figure 2. Process of the 3D position estimation algorithm

2.2. Simulations

To evaluate the estimation performance of the proposed method, a series of simulations were performed for two different application scenarios.

First, to use the proposed method for a moving tumor setup before treatment, similar to CBCT use, an interdimensional correlation model was built using full-rotation projection data assumed to have been acquired from

a CBCT scan. The same model parameters were then retrospectively applied to all projection data to estimate their 3D position. Second, for the purpose of real-time target position monitoring during gating or tracking delivery of either VMAT or IMRT, an interdimensional correlation model was initialized using a limited range of angular projection data. This model was updated on-the-fly each time new projection data were added, and then applied to estimate the 3D position of the new projection data.

The ground truth data used for the simulation were the 3D target positions of 160 thoracic/abdominal trajectories from 46 patients. The targets were fiducial gold markers inserted near to the tumors. The time spent acquiring each trajectory varied from 8 to 110 min. The 3D position data of the trajectories were obtained from the CyberKnife Synchrony system at Georgetown University Hospital. The 3D positions were accurately calculated using an analytic formula for dual imaging systems.[17] For the retrospective estimation, each trajectory was divided into 60-s segments to simulate 60-s CBCT scanning. Hence, we obtained 4893 60-s segmented trajectories and 4893 simulated CBCT datasets. The mean and maximum range of motion for all 60-s segmented trajectories were calculated to be 2.5 mm and 26.3 mm (LR), 6.9 mm and 56.6 mm (SI), and 3.3 mm and 37.3 mm (AP), respectively.

To acquire CBCT projection data numerically, we applied Eq. (1) to the 3D target position data. The simulated CBCT scanning conditions are shown in Fig. 3(a). The imager rotates 360° counter-clockwise (CCW) in 60 s, starting with a horizontally aligned OBI system. An imaging frame rate of 10 Hz was assumed, resulting in 600 projections per scan. The correlation model parameters were determined once using all 600 projected positions as training data, and then the same parameters were retrospectively applied to all projected positions to estimate the 3D target trajectory during CBCT scanning.

For the on-the-fly application of the estimation method, realistic treatment cases of VMAT and IMRT were simulated. The VMAT was assumed to consist of full-rotation treatment, with delivery starting at a gantry angle of 180° in the International Electrotechnical Commission (IEC) gantry scale and the rotation proceeding at 6°/s CCW. Thus, in regard to the kV imaging condition, the VMAT simulation was the same as the retrospective CBCT simulation, that is, one rotation took 60 s with a 10 Hz imaging rate. The geometry of the gantry and imaging system for the VMAT is shown in Fig. 3(b). The total number of trajectory segments was 4893 with 600 projections per trajectory, as for the retrospective simulation. For the conventional IMRT case, a treatment plan of six stationary

IMRT fields was simulated. The beam-on time of each field was 20 s. The angles of the kV imaging source at the six beam-on positions were θ_i = 30°, 90°, 150°, 210°, 270°, and 330°, as shown in Fig. 3(c). The beam-to-beam gantry rotation speed was assumed to be 6°/s. Therefore, the total imaging duration for one IMRT treatment was 175 s (initial imaging while rotating 0–30°, 20-s imaging at 30° during delivery of the first beam, imaging while rotating of 30–90°, 20-s imaging at 90° during delivery of the second beam, and so on). As a result, 1750 projection data were obtained. A total of 1618 segmented trajectories were recorded in this simulation.

In the VMAT and IMRT delivery, the 3D target position estimation first established the interdimensional model parameters from the first 25 projection data, obtained over 0–15° of the kV imaging source during 2.5 s. Each time new projection data were added, the model parameters were updated using the whole projection dataset, and the updated parameters were applied to estimate the 3D position of the new projection data. The update and estimation process was repeated for all data obtained from the 26th projection onwards. Only the simple linear correlation model was applied to evaluate the performance of on-the-fly estimation in the VMAT and IMRT cases.

The accuracy of the trajectory estimations was evaluated using the maximum error and root-mean-square error (RMSE). The RMSE of a trajectory in the LR direction, for example, was calculated as:

$$RMSE_j(x) = \sqrt{\frac{\sum_i (x_{ij}^{est} - x_{ij}^{act})^2}{N}}_{\in i,j}, \tag{7}$$

where i depicts the projection number in the trajectory (i = 1, 2, ⋯, N) and j refers to the trajectory number (j = 1, 2, ⋯, M).

The maximum error is the largest absolute difference in terms of 3D distance between the estimated target position X^{est} and the actual target position X^{act}.

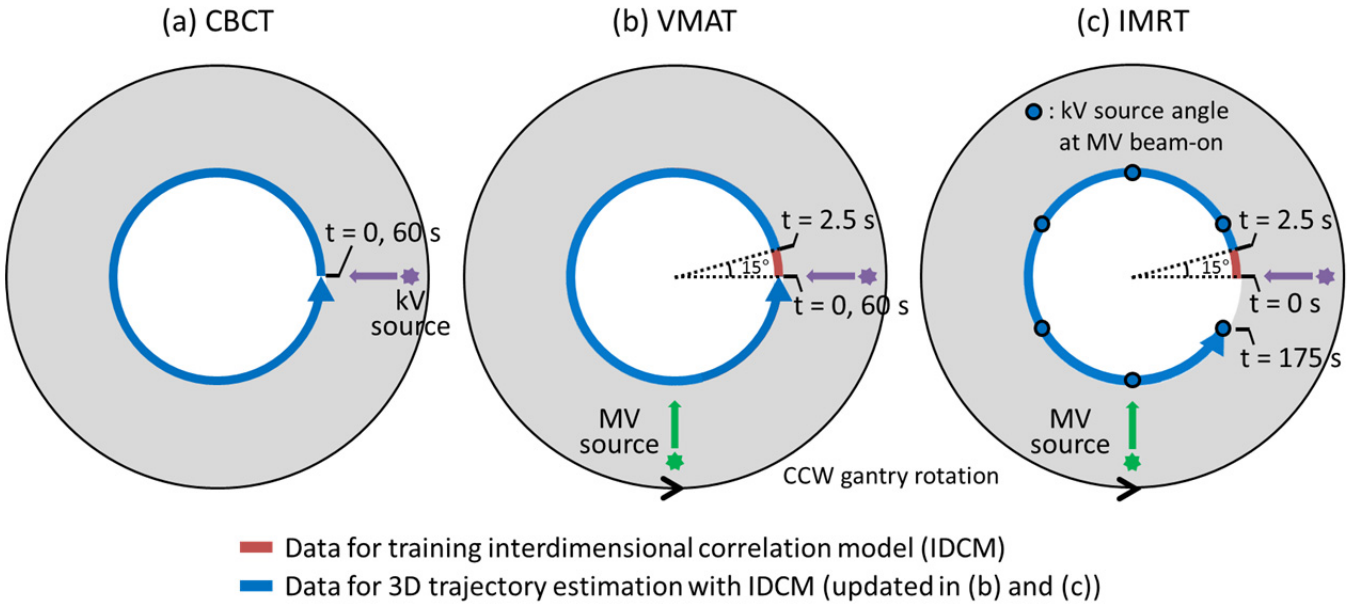

Figure 3. Geometries and scenarios of the kV imaging system for (a) retrospective CBCT simulation and on-the-fly simulation of (b) a full-rotation VMAT and (c) six-field IMRT. Note that the gantry angle (MV beam direction) began at 180° in the IEC 1217 scale, from which a kV imaging source was located laterally with 90° offset at 0° in the scale of this study, and rotated CCW. In (a), the inner red circle indicates the training model parameters using all of the projection data from one CBCT scanning. After model parameter training, 3D trajectory estimation was performed with all projection data using the model parameters already calculated, represented as the outer blue circle. In (b) and (c), the projection data on the red line (first 15° gantry rotation during 0–2.5 s) were only used for model parameter training. After 2.5 s training, the 3D position estimation began updating the model parameters using the accumulated data on the blue line.

III. RESULTS

3.1. Retrospective estimation for CBCT scanning

Fig. 4 shows the reconstructed target trajectories given by the interdimensional correlation models in (a) simple linear form and (b) state-augmented form in comparison with the actual trajectory of a well-behaved case. The high interdimensional linear correlation between the SI motion and AP or LR motions in this cases results in excellent estimations of AP and LR trajectories. In contrast, Fig. 5 shows a challenging case in which the periodicity of lung motion is seriously broken. In this instance, both correlation models give large estimation errors in the LR and AP directions. There could be several reasons for this poor estimation. During the initial 10 s, in particular, a noticeably large movement occurred in the LR direction, apparently due to patient body movement. Interdimensional correlation modeling cannot recover such a huge discrepancy. The overall respiratory pattern was irregular, which further reduced the interdimensional correlations and increased the estimation error. In addition, because the range of motion in the SI direction was smaller than that of either the AP or LR motion, small amounts of noise in the SI motion can propagate into large errors in the AP or LR motions. This should be considered a limitation of our method. However, in most cases of normal breathing, the range of motion in the SI direction is two or three times larger than that in either the AP or LR direction, as shown in Fig. 4.

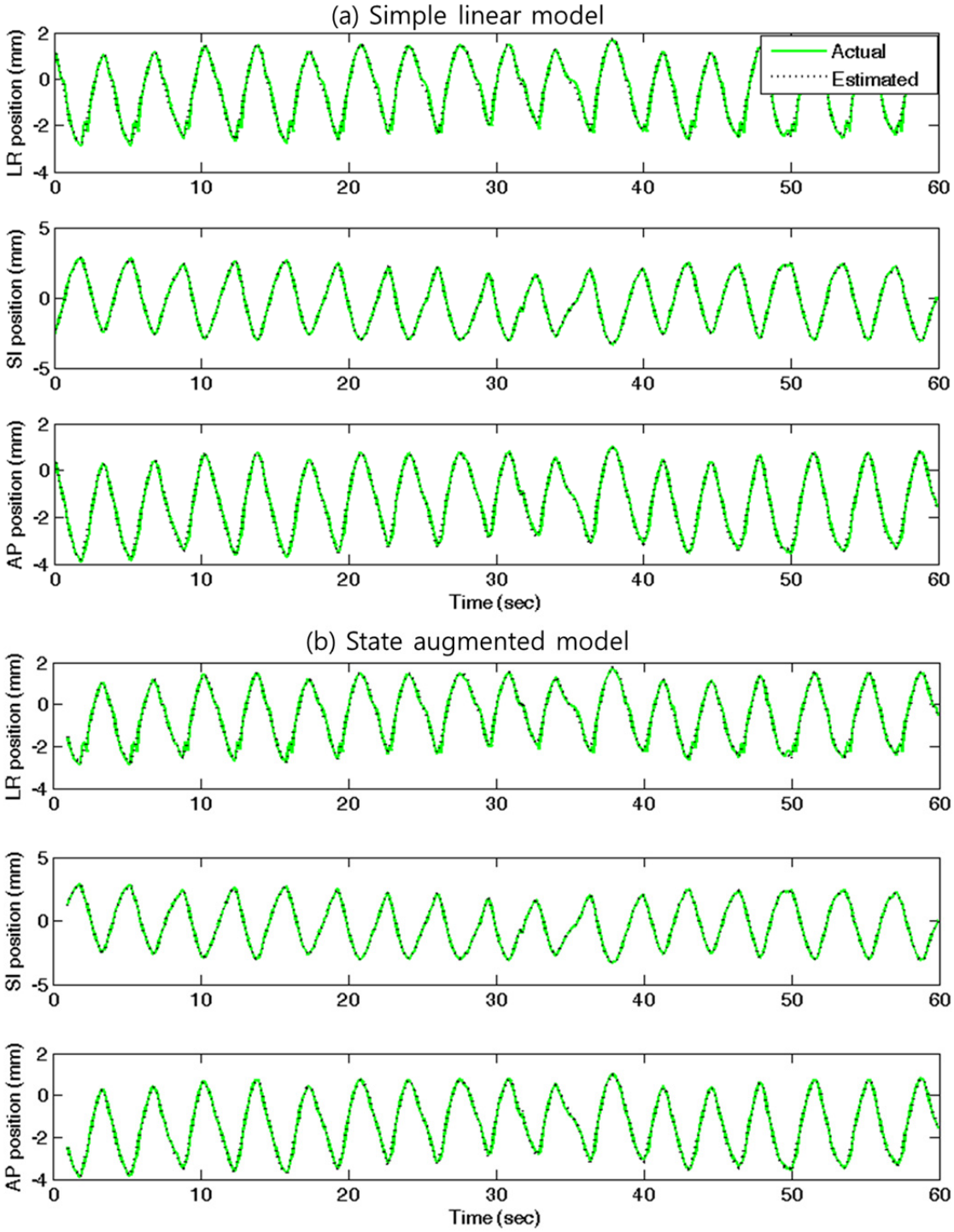

255 **Figure 4.** Estimated target trajectory (black dotted line) and actual target trajectory (green) of a typical well-estimated case applying (a) simple linear modeling (3D RMSE: 0.20 mm) and (b) state-augmented modeling (3D RMSE: 0.17 mm).

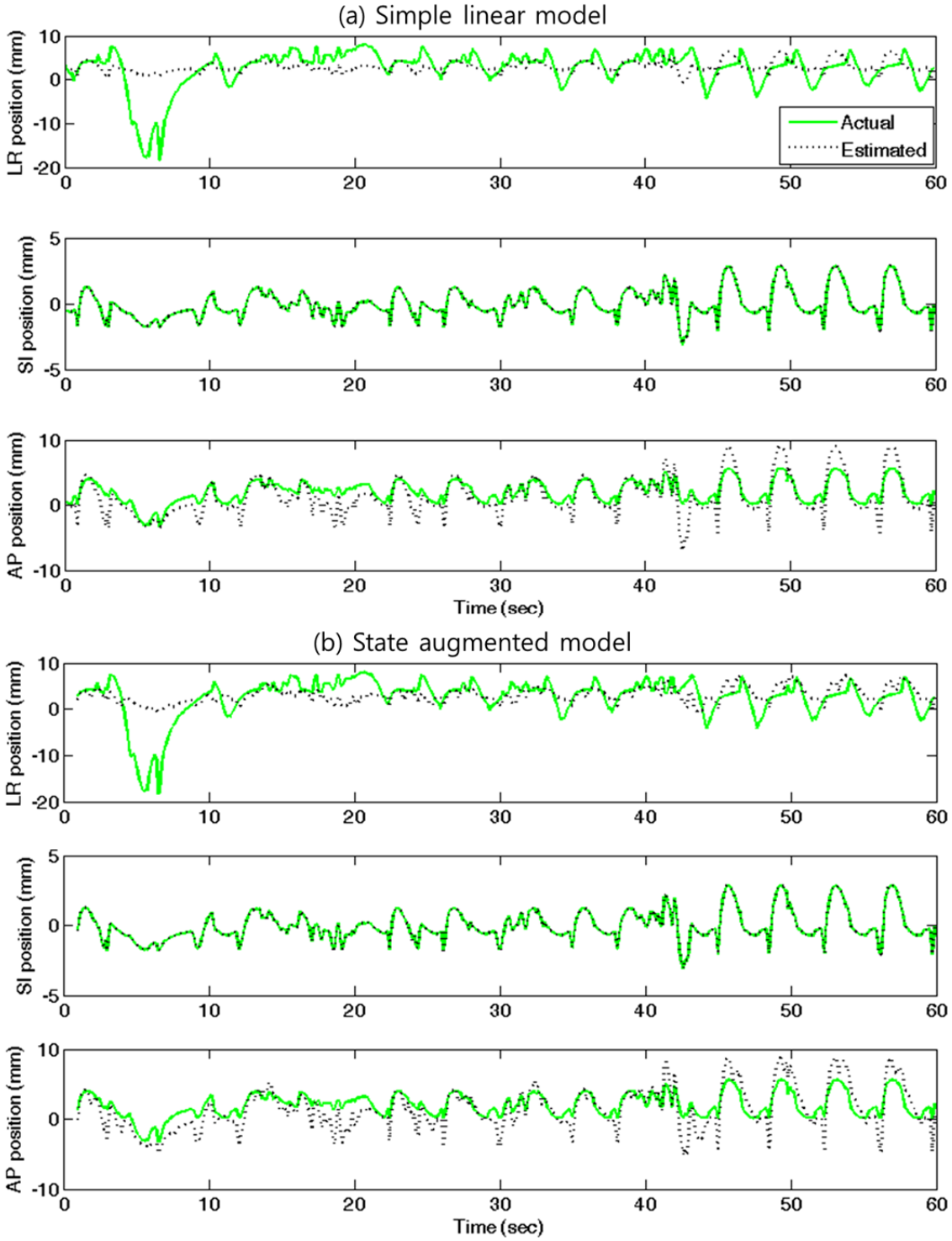

260 **Figure 5.** Estimated target trajectory (black dotted line) and actual target trajectory (green) applying (a) simple linear form (3D RMSE: 4.40 mm) and (b) state-augmented form for the maximum 3D RMSE case (3D RMSE: 4.33 mm).

Figs. 6 and 7 show the distribution of RMSE for the sampled points in all of the trajectories. The red solid line in the box represents the median values of the RMSE distribution. The upper line of the box indicates the 75th percentile, and the lower line indicates the 25th percentile. The whiskers extend to the most extreme data points that are not considered outliers. The outliers are individually plotted as red daggers. The upper whisker represents $q_{75} + w(q_{75} - q_{25})$ and the lower whisker represents $q_{25} - w\ (q_{75} - q_{25})$, where q_{25} and q_{75} are the 25th and 75th percentiles, respectively. The whisker length w was set to 1.5, which corresponds to approximately $\pm 2.7\sigma$ and 99.3% coverage if the data are normally distributed.

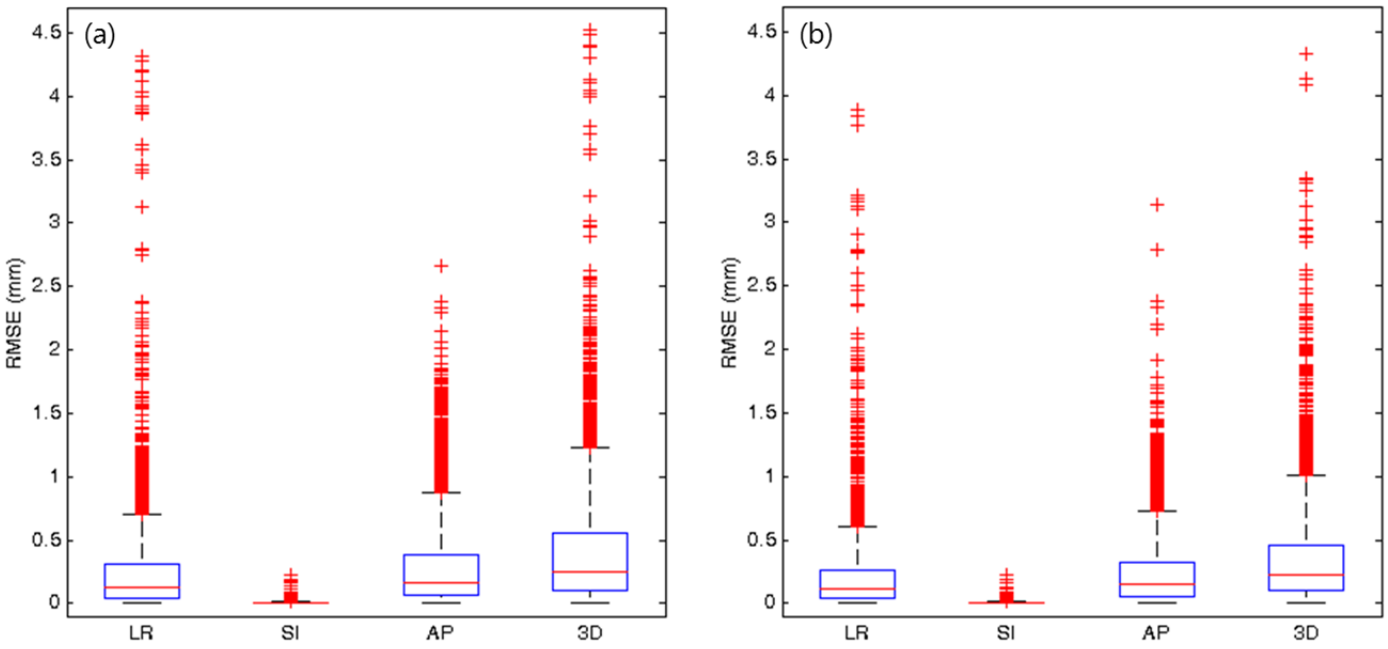

Figure 6. Distribution of RMSE of trajectories using (a) the simple linear model and (b) state-augmented model.

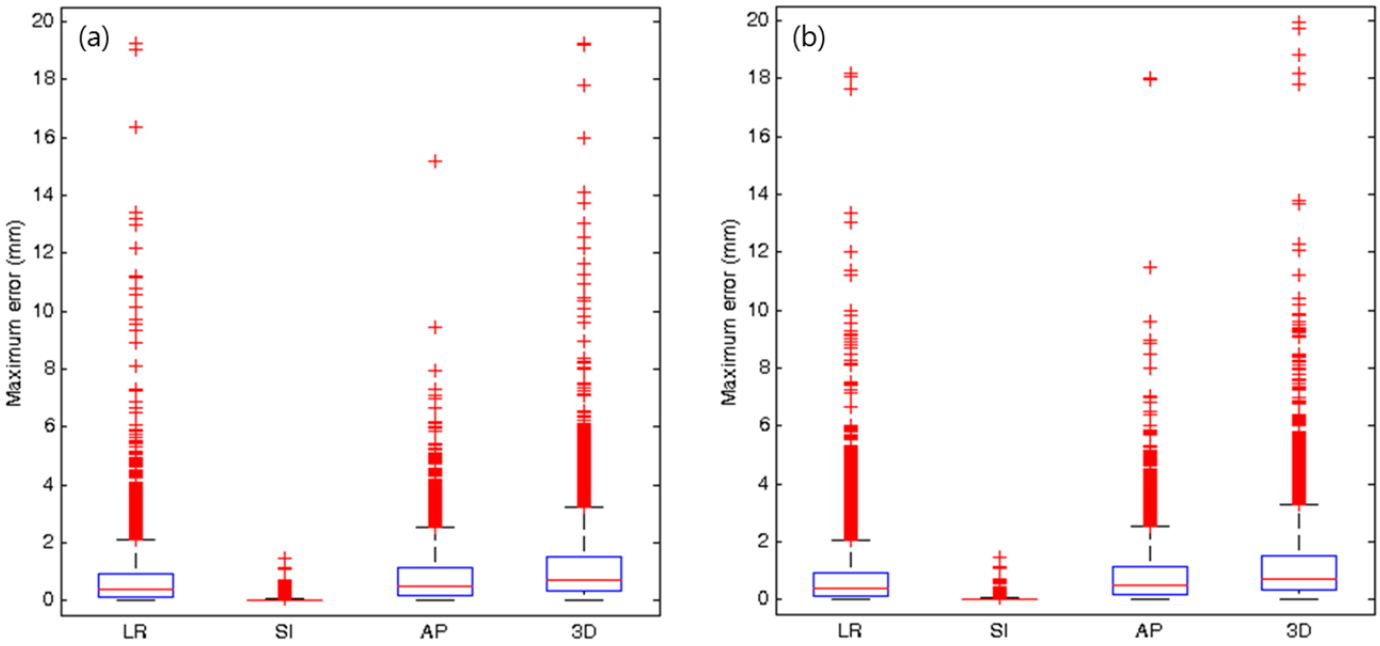

Figure 7. Distribution of maximum error values of all points using (a) the simple linear model and (b) state-augmented model.

Table I summarizes the performance of the interdimensional correlation models when using CBCT projection data to reconstruct target trajectories in each direction in terms of RMSE and maximum absolute error. This table also includes the lower bounds of the 95th percentiles of RMSE and maximum errors in consideration of signals away from noise.

Table I. Mean and 95th percentile RMSE of the estimated trajectories and 95th percentile maximum error of estimated target points according to the simple linear model and state-augmented model.

	Mean RMSE (mm)				95% RMSE (mm)				95% maximum error (mm)			
	LR	SI	AP	3D	LR	SI	AP	3D	LR	SI	AP	3D
Simple linear	0.24	0.0065	0.29	0.41	0.78	0.022	1.05	1.30	2.47	0.0079	2.79	3.55
State-augmented	0.21	0.0065	0.24	0.35	0.67	0.022	0.78	1.03	2.44	0.079	2.74	3.59

Table II summarizes the percentage of estimated trajectories within a specified margin of error. The 3D RMSE was less than 1 mm in 90.8% (simple linear model) and 94.7% (state-augmented model) of all trajectories. The state-augmented model demonstrated slightly higher performance. The 3D RMSE was less than 2 mm for approximately 99% of all cases. Approximately 61% of the thoracic/abdominal cases demonstrated a maximum 3D error of less than 1 mm, and approximately 84% of the cases demonstrated maximum 3D errors of less than 2 mm.

Table II. Percentage of reconstructed trajectories with 3D RMSE and maximum errors of less than 1 mm and less than 2 mm.

	3D RMSE		3D maximum error	
	<1 mm	<2 mm	<1 mm	<2 mm
Simple linear (%)	90.8	98.8	61.2	83.6
State-augmented (%)	94.7	99.1	61.5	83.9

In Fig. 8, we compare the performance of the simple linear model and the state-augmented model by plotting the RMSE values for all of the estimated trajectories. The results are generally below the red line, which has a slope of 1, indicating that the state-augmented model gave more accurate estimates.

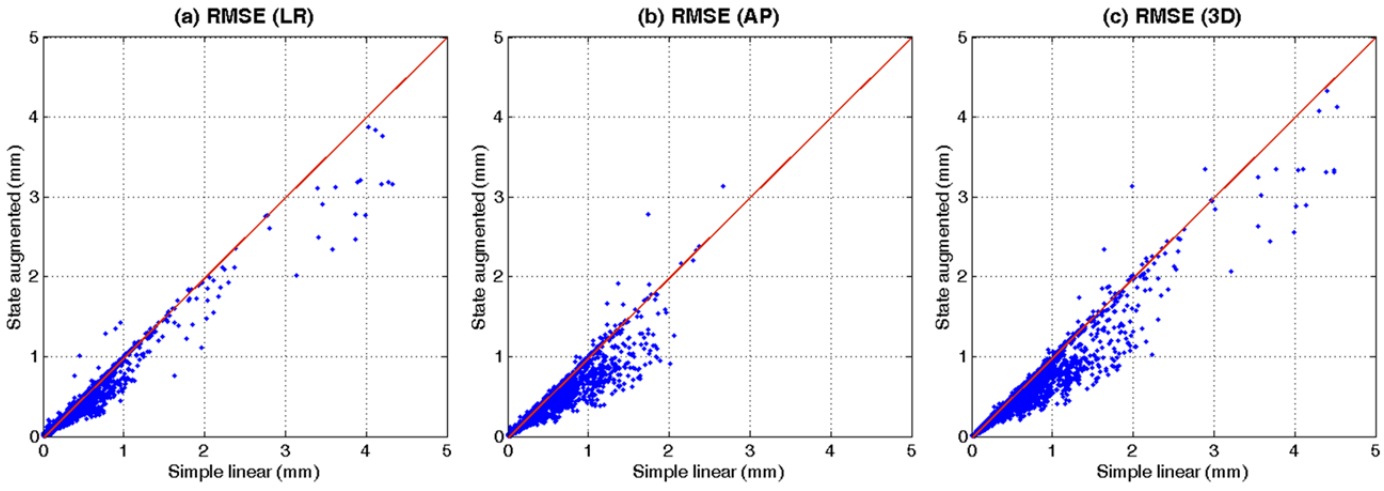

Figure 8. Scatter plots of RMSE of estimated trajectories determined using the state-augmented model and simple linear model in (a) the LR direction, (b) the AP direction, and (c) 3D.

3.2. On-the-fly estimation for arc or stationary treatment cases

The on-the-fly estimation method was applied to both VMAT and IMRT treatments. The average estimation errors of the resulting 3D trajectory segments are shown as a function of time and kV imaging source angle in Fig. 9. The estimation started after the acquisition of 25 training data during the first 2.5 s. The errors at the beginning of the estimation were quite substantial, and then rapidly decreased with time. This can be explained as follows. First, to build reliable model parameters, the correlation model needs a set of projection positions over at least one breathing cycle, which takes around 4–5 s. As can be seen in Fig. 9, after around 5 s, the estimation error decreased considerably. Second, the estimation error along the projection direction was initially high because of the limitations of the monoscopic approach. It can also be observed from Fig. 9 that, because the kV imaging source started to rotate from 0°, the unresolved lateral (LR) motion produced relatively large errors compared to the AP direction. These unresolved errors decreased rapidly until around 10 s, which indicates that projection data over an angle of 60° are needed to overcome the uncertainty of unresolved motion in the monoscopic approach. For the VMAT treatments, 135 projection data over a rotated angle of 81° were needed to reduce the average 3D estimation error to less than the value of the average retrospective estimation error (0.33 mm). In the conventional IMRT simulation, 349 projection data and a rotation angle of 89.4° were needed for the same accuracy. Therefore, we can conservatively presume that the projected positions acquired over an angular span of 90° are necessary for reliable 3D position estimation. In real treatment applications, pretreatment imaging for 90° gantry rotation would be recommended for training the interdimensional correlation model.

In the IMRT simulation, the projection data were acquired over a 30° rotation before the first beam delivery, and then the projection angle was held for 20 s while the MV beam was on, which caused the estimation error to increase slowly over the first beam delivery (5–25 s), as can be seen in Fig. 9(b).

Unlike the VMAT case, the estimation error of the IMRT case increased over the entire treatment time (5–175 s), even after more than 90° angular projection data had been acquired. This is likely to be because the delivery time of the IMRT was three times that of the VMAT and all projection data were used to determine the model parameters. The correlation model is likely to be stable over a VMAT delivery time of around 60 s, but begins to change over the 180 s of IMRT delivery, indicating that the training data for determining the model parameters should somehow be limited to the most recent data to effectively reflect changes in the respiratory pattern over time, a kind of baseline drift.

To better understand the impact of the time interval of training data on the estimation performance of the model, additional VMAT and IMRT simulations were performed. Projection data over an angular range of 90° were assumed to have been acquired before the start of the estimation, as well as before the start of the beam delivery of each therapy. The model parameters were updated on-the-fly using only the most recently acquired projection data over a 90° range, rather than including the whole projection dataset. As a result, the VMAT training data included only the most recent 150 projection data acquired over an angle of 90° during a 15-s period, whereas the training data for the IMRT simulation varied to include the most recent 150–350 projection data because of the 20-s beam delivery interval of stationary IMRT. The estimation errors averaged over all trajectory segments are shown as a function of time and kV imaging source angle in Fig. 9(c) and (d). It can be seen that the estimation began after the pre-acquisition of 90°-ranged projection data, and that the error was small at the beginning and constant over the entire duration of beam delivery. The 3D RMSE of VMAT and IMRT, averaged over all the trajectory segments, was 0.42 mm and 0.45 mm, respectively, which is comparable to the 0.41 mm of the retrospective CBCT case (Table I).

Finally, we also investigated how fast the estimation error would increase without updating the model parameters. This simulation assumed that, after establishing the model parameters with 90° rotational projections, the estimation continued for 10 min with the same model parameters. The results indicate that the mean 3D RMSE increased linearly at a rate of 0.07 mm per minute, reaching 1.1 mm after 10 min.

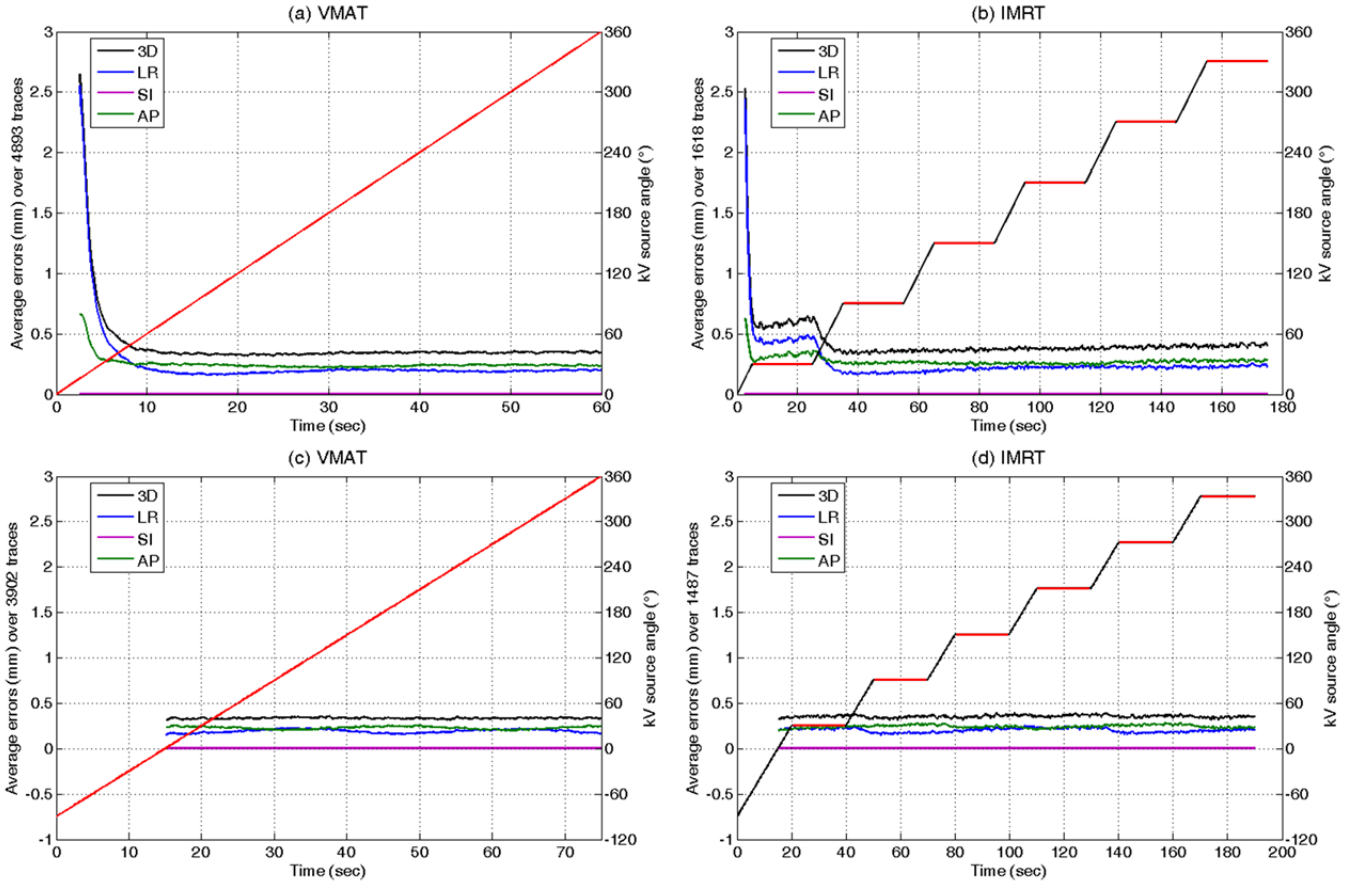

Figure 9. Estimation errors as a function of time and kV imaging source angle, averaged over all the simulation trajectories for (a) VMAT and (b) IMRT treatment cases with 2.5-s training data. (c) and (d) show the average error of trajectory estimation with model parameters trained with 150 s/90° pre-treatment imaging data and updated with the most recent 150–350 projection data over a 90° range. The diagonal red lines on the graphs represent kV source angles (θ_i) when the treatment (MV) beam was on. In the IMRT cases, (b) and (d), the black lines between red lines represent beam-to-beam gantry rotation between six IMRT fields.

IV. DISCUSSION

In this study, we developed algorithms for estimating the 3D target position of thoracic/abdominal tumors from CBCT projection images. The proposed method uses interdimensional correlations between the LR, AP, and SI motions of the target and does not require external surrogates to estimate the target position. In addition, our method does not require probability distribution functions (PDF) of the motion, such as 3D Gaussian PDF approaches or the Bayesian approach. Breathing motion can be biomechanically interpreted as the repeated contraction and relaxation of the diaphragm and intercostal muscles. During inspiration, the diaphragm moves downward to increase the volume of the thoracic cavity, and the intercostal muscles pull the ribs up to expand the rib cage and further increase the volume. During expiration, the diaphragm and intercostal muscles relax, which returns the thoracic cavity to its original volume. The 3D motion of each respiration-induced target movement is correlated during these repetitive processes, and this correlation serves as the basis of our interdimensional model. Our approach estimates a target motion in thoracic and abdominal sites, in which the respiratory cycle is assumed to be generally periodic.

The accuracy of the proposed estimation appears to be comparable to a more sophisticated estimation method based on 3D Gaussian PDFs or the Bayesian approach. The mean 3D RMSE values given by the Bayesian approach were reported to be 0.65 mm and 0.40 mm in phantom experiments on the lung and pancreas, respectively.[4] A 3D Gaussian PDF using the same thoracic/abdominal data as in this study found the mean 3D RMSE for thoracic/abdominal motion to be 0.17 mm,[12] whereas the mean 3D RMSE in this study was 0.35 mm. The Gaussian PDF method produced estimation results of higher accuracy because, in addition to interdimensional motion correlations, it identifies and utilizes motion confined to a single line or on a single plane. Even though more sophisticated methods provide higher overall estimation accuracy, one of the big advantages of the proposed method is its simplicity and estimation speed, which would enhance real-time tumor tracking by substantially reducing the computation time. The proposed method would be particularly advantageous to IGRT with CBCT imaging during treatments such as VMAT.

Using MATLAB (Mathworks, Natick, MA) on a typical desktop PC environment, the computation time to estimate an entire CBCT trajectory composed of 600 projection data points in the retrospective CBCT simulation, averaged over the 4,893 trajectory segments, was 0.007 s for the interdimensional correlation method, some 200

times faster than the 1.53 s of the 3D Gaussian probability-based method. A recent implementation of the 3D Gaussian probability-based method in a fully integrated real-time 3D tumor monitoring system for radiotherapy reported a latency of 350 ms for the processes of kV imaging, marker segmentation, position estimation, and multileaf collimator adjustment.[18] Thus, the time required for the position estimation itself would not affect the real-time target position monitoring under efficient optimization of the algorithm. Although the error associated with the latency in real-time application can be effectively mitigated by applying prediction algorithms, it is important for overall tracking accuracy to minimize the latency first as small as possible. We expect the interdimensional correlation approach could further reduce the overall latency by ~50 ms. However, it should be further investigated whether this latency time-saving will be significant or not, with taking account of the estimation performances. Along with this fast estimation speed, the accuracy of the simulations for on-the-fly applications to VMAT and IMRT demonstrates the feasibility of our method in real-time application.

In this study, the method was validated by performing simulation studies of 3D tumor trajectories from which the rotationally and sequentially projected target positions were calculated according to a typical OBI geometric configuration. Assuming that the fiducial marker was located at the tumor and the projection positions were measured during CBCT scanning, the estimation model was applied to the projection positions to reconstruct their 3D target position. By comparison with the 3D tumor trajectory assumed to be the ground truth, the reconstructed 3D target positions given by the proposed estimation method were validated.

The proposed method was developed for applications using implanted fiducial markers as surrogates of the tumor position. However, implanted marker-based tumor tracking has several well-known limitations: for lung tumors, there is a risk of pneumothorax with subcutaneous implantation[19] or migration issues with endobronchial marker placement[20]; for liver and pancreas tumors, implanted fiducial markers are generally imperative for tumor tracking, because the tumor contrast is poor as a result of a lack of soft tissue contrast. Direct tumor segmentation can overcome this issue, although there are various challenges in dealing with tumors other than solid lung tumors surrounded by low-density lung tissue,[21, 22] or a well-demarcated Lipiodol near liver tumors[23].

For the clinical implementation of the proposed method, several issues still need to be addressed. First, accurate identification of the fiducial marker on the projected image is challenging when it is obscured by dense bony

structures. Therefore, efficient segmentation and an effective method for dealing with marker search failures are necessary. Second, because fiducial markers can only be used as a surrogate of the tumor position, the geometric offset of the markers from the tumor should be taken into account. Third, there will be a time delay associated with OBI image acquisition, marker identification, and the estimation model. As the overall latency may not be negligible, a robust prediction method that compensates for the system latency may be needed for respiratory gating or tumor tracking applications. Finally, the extra imaging dose associated with continuing X-ray imaging should also be optimized through a trade-off between the improved accuracy given by increasing the imaging frequency and the associated risks. A recent measurement study[24] reported an imaging dose of 0.4–2.6 cGy per CBCT scan, which can be neglected compared to a large amount of the prescription dose of SBRT delivered in 3–5 fractions.

In this study, the imaging frame rate was fixed at 10 Hz. Imaging frequency (f s^{-1}), in combination with the time window (t s) and the number of training data points ($n = f \times t$) used for the model parameters estimation, affects the accuracy associated with the estimation models using an interdimensional correlation of this study and an internal-external correlation between internal target position and external optical surrogate motion[5]. You can easily see that n (>10) would be enough for the simple linear square estimation to determine at most 2 or 3 model parameters. The time window may be adequately chosen if it covers several breathing cycles, around 10–20 s. Therefore, imaging frequency of 1–0.5 Hz would be appropriate. The time window also affects the accuracy of the on-the -fly estimation because it determines how often the correlation model is updated. Therefore, it is intimately related with how rapidly the correlation, i.e. the breathing pattern, would change. In most cases, changes in breathing pattern like baseline shift would be expected to happen eventually minute-by-minute rather than second-by-second. Indeed, at the end of the results section we already estimated how fast the estimation error would increase without updating the model, i.e., how quickly the correlation can change, and founded that the 3D RMSE was increasing at a rate of 0.07mm per minute, reaching 1.1 mm after 10 min. This fact was also confirmed with our pervious study[5], a longer imaging interval increases the estimation error gradually because the wider time window for the model parameters estimation using a fixed number of training data (n = 20) slows down the model adaptation to the temporal change in the correlation, i.e., changes in breathing pattern such as baseline drift. This response delay of the

model adaptation adds ~0.2 mm on the 3D estimation error up to the 10-s imaging interval with the 200-s time window.

Nonetheless, there exists a residual error in the motion estimation by the proposed method, and such a limitation is indeed intrinsic to all the monoscopic approaches. Stereoscopic imaging systems such as Cyberknife and ExacTrac do not suffer from this kind of problem, which is caused by imaging system alignment. However, this limitation can be somewhat mitigated by varying the projection angles, because the relationship between LR/AP motion and SI motion for a certain patient remains relatively stable from breathing cycle to cycle although there may be variations in the period length and inspiration depth of each breathing cycle. Thus, the unresolved motion in one direction becomes detectable by varying the projection angle, as in CBCT acquisition. Our earlier work,[3] which compared the accuracy of target position estimation using an internal–external correlation model for monoscopic imaging and stereoscopic imaging, showed that the residual error of the model was much larger than the error induced by different imaging systems.

As summarized in Table II, 99% of the reconstructed points in the trajectories have 3D RMSEs of less than 2 mm. Because the dosimetric error in the radiation treatment is more closely associated with the RMSE error than with the maximum error, we believe that the proposed model would provide efficient real-time motion tracking for dose management. The proposed model is based on the assumption that there exists a high linear correlation between directional motions. This assumption is validated in Fig. 10 and Table III.

Fig. 10 shows the histogram of interdimensional correlation coefficients, and a strong correlation is evident. More than half of the trajectories have correlation coefficients larger than 0.9, as summarized in Table III.

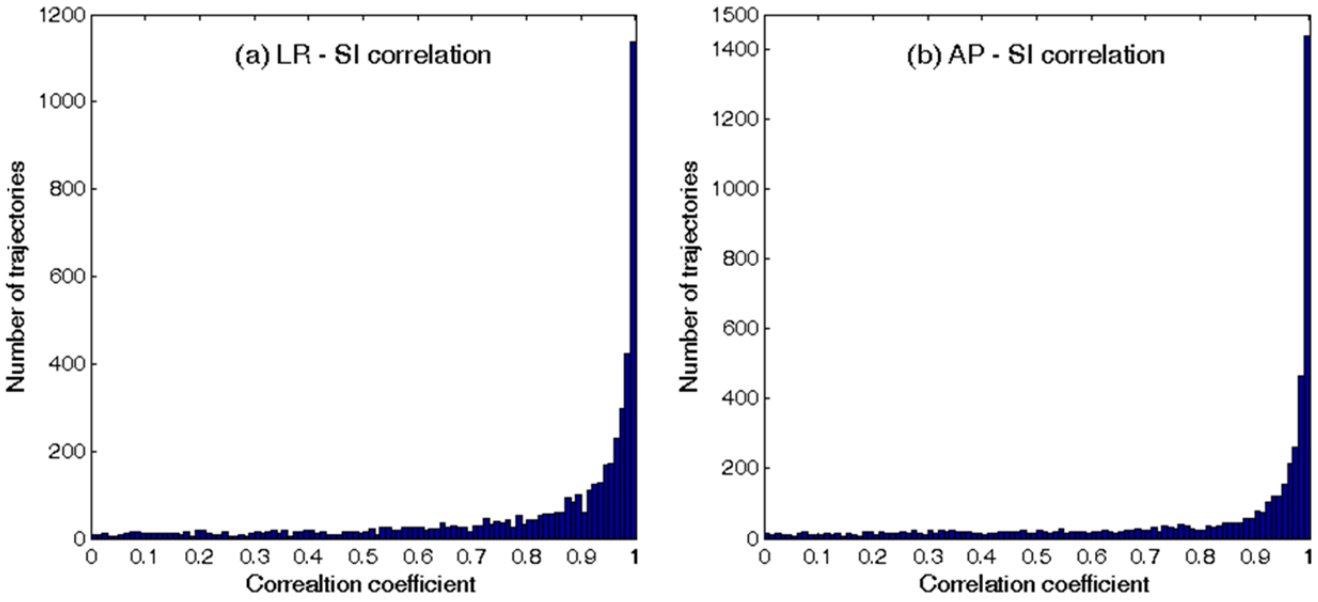

Figure 10. Distribution of absolute correlation coefficients between the (a) LR and SI directions and (b) AP and SI directions.

Table III. Percentage of trajectories with correlation coefficients >0.5, >0.7, or >0.9.

	LR – SI (%)	AP – SI (%)
> 0.5	87.9	84.7
> 0.7	78.8	76.5
> 0.9	58.2	62.0

Suh et al.[17] reported similar high linear correlation by using principal component analysis (PCA) with the same trajectory dataset, and demonstrated PCA can be used to separate nonlinear and hysteresis motion from linear motion, even though it cannot be used to differentiate between motion linearity and hysteresis. In this study, to improve estimation accuracy for hysteresis we implemented a state augmented method with a first order approximation. However the state augmented method resulted in a small gain in the estimation accuracy (4% in < 1 mm 3D RMSE in Table II), suggesting that the motion hysteresis is complex with contributions of higher order.

It is worth mentioning the effect of time lag on the accuracy of position estimation in the state-augmented model. We compared the mean 3D RMSEs of all the reconstructed trajectories with various time lags, and chose the

optimum time lag of 0.6 s. However, varying the time lag from 0.2–1 s produced a difference of less than 0.01 mm in terms of 3D RMSE. This is negligible compared to the planning target volume (PTV) margin, which is about 5 mm in standard thoracic/abdominal cases.

As the initial large LR motion of the trajectory in Fig. 5 is unlikely to be caused by respiratory motion, the proposed method, which assumes a periodic and inter-dimensionally correlated respiratory motion, does not work well in this case. For any monoscopic estimation method, it is challenging to estimate the target positions accurately in cases where unpredictable sudden motion changes occur during CBCT imaging. In radiation treatment, a practical strategy to deal with such irregular breathing or sudden motion changes is to hold the beam delivery when the target position is outside a certain confidence interval (CI). For example, the 95th percentile of the 2D RMSE of $\hat{\mathbf{p}}(x_p, y_p)$ could be used for the CI value; in the present study, this value was calculated to be 1.33 mm in the simple linear model.

In addition, a visual comparison of the estimated projected trajectory with the measured one on the imager plane can provide an immediate and strongly intuitive evaluation of the estimation performance of the model. For example, Fig. 11 shows the actual and estimated projection data. This real-time visual comparison during treatment can be a useful cue for therapists to interrupt the beam delivery when a large discrepancy appears on the display.

Finally, with the help of a marker segmentation tool, on-line application of the retrospective estimation immediately after a CBCT acquisition can provide tumor position and motion information. In respiratory motion-inclusive approach, the mean tumor position can be used for moving tumor setup, or in respiratory gated treatment the end-exhale tumor location can be used for alignment of mobile tumor. Furthermore the motion information allows calculation of appropriate margins in motion-inclusive treatment, or evaluation of respiratory regularity before treatment and individualization of the gating window to accommodate daily baseline shifts.

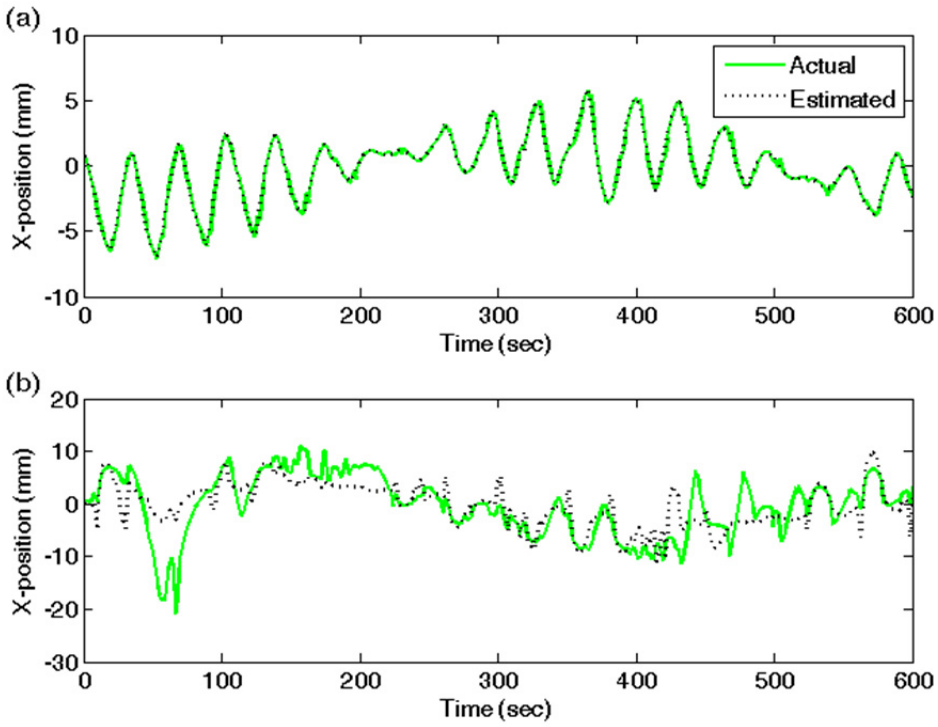

Figure 11. Projected position $\hat{x}_p$ of estimated target trajectory (black dotted line) and actual projection data x_p (green) of (a) the typical case shown in Fig. 4 and (b) the case of maximum 3D RMSE shown in Fig. 5.

5. CONCLUSION

For respiratory motion that is fairly periodic and exhibits a high intercorrelation between directional components, the proposed method was shown to effectively estimate the tumor motion from CBCT projection data. The method does not require external surrogates or computationally expensive probabilistic models, and has the potential to be used for both retrospective IGRT with CBCT projection images and real-time target position monitoring for respiratory gating or tracking.

ACKWOWLEDGMENTS

This work was supported by the National Research Foundation of Korea (NRF) grant funded by the Korea government (MSIP) (No. 2015038710). The authors declared no potential conflict of interest with respect to the research, authorship, and/or publication of this paper.

Reference:

[1] L. Xing, B. Thorndyke, E. Schreibmann, Y. Yang, T.F. Li, G.Y. Kim, G. Luxton, A. Koong, "Overview of image-guided radiation therapy," Medical dosimetry : official journal of the American Association of Medical Dosimetrists **31**, 91-112 (2006).

[2] H. Pan, D.R. Simpson, L.K. Mell, A.J. Mundt, J.D. Lawson, "A Survey of Stereotactic Body Radiotherapy Use in the United States," Cancer **117**, 4566-4572 (2011).

[3] A.S.o.R. Technologists, "Radiation therapy staffing and workplace survey 2014: A nationwide survey of radiation therapy managers," (Accessed April 22, 2016).

[4] D. Jones, "ICRU Report 50—Prescribing, Recording and Reporting Photon Beam Therapy," Medical Physics **21**, 833-834 (1994).

[5] B. Cho, P.R. Poulsen, P.J. Keall, "Real-time tumor tracking using sequential kV imaging combined with respiratory monitoring: a general framework applicable to commonly used IGRT systems," Physics in medicine and biology **55**, 3299-3316 (2010).

[6] R. Li, B.P. Fahimian, L. Xing, "A Bayesian approach to real-time 3D tumor localization via monoscopic x-ray imaging during treatment delivery," Medical Physics **38**, 4205 (2011).

[7] T.E. Marchant, A.M. Amer, C.J. Moore, "Measurement of inter and intra fraction organ motion in radiotherapy using cone beam CT projection images," Physics in medicine and biology **53**, 1087-1098 (2008).

[8] R.I. Berbeco, S.B. Jiang, G.C. Sharp, G.T. Chen, H. Mostafavi, H. Shirato, "Integrated radiotherapy imaging system (IRIS): design considerations of tumour tracking with linac gantry-mounted diagnostic x-ray systems with flat-panel detectors," Physics in medicine and biology **49**, 243-255 (2004).

[9] B. Cho, Y. Suh, S. Dieterich, P.J. Keall, "A monoscopic method for real-time tumour tracking using combined occasional x-ray imaging and continuous respiratory monitoring," Physics in medicine and biology **53**, 2837-2855 (2008).

[10] J.H. Lewis, R. Li, W.T. Watkins, J.D. Lawson, W.P. Segars, L.I. Cervino, W.Y. Song, S.B. Jiang, "Markerless lung tumor tracking and trajectory reconstruction using rotational cone-beam projections: a feasibility study," Physics in medicine and biology **55**, 2505-2522 (2010).

[11] R. Li, X. Jia, J.H. Lewis, X. Gu, M. Folkerts, C. Men, S.B. Jiang, "Real-time volumetric image reconstruction and 3D tumor localization based on a single x-ray projection image for lung cancer radiotherapy," Med Phys **37**, 2822-2826 (2010).

[12] P.R. Poulsen, B. Cho, P.J. Keall, "A method to estimate mean position, motion magnitude, motion correlation, and trajectory of a tumor from cone-beam CT projections for image-guided radiotherapy," International journal of radiation oncology, biology, physics **72**, 1587-1596 (2008).

[13] N. Becker, W.L. Smith, S. Quirk, I. Kay, "Using cone-beam CT projection images to estimate the average and complete trajectory of a fiducial marker moving with respiration," Physics in medicine and biology **55**, 7439-7452 (2010).

[14] J.C. Park, S.H. Park, J.H. Kim, S.M. Yoon, S.Y. Song, Z. Liu, B. Song, K. Kauweloa, M.J. Webster, A. Sandhu, L.K. Mell, S.B. Jiang, A.J. Mundt, W.Y. Song, "Liver motion during cone beam computed tomography guided stereotactic body radiation therapy," Med Phys **39**, 6431-6442 (2012).

[15] B. Cho, P. Poulsen, D. Ruan, A. Sawant, P.J. Keall, "Experimental investigation of a general real-time 3D target localization method using sequential kV imaging combined with respiratory monitoring," Physics in medicine and biology **57**, 7395-7407 (2012).

[16] D. Ruan, J.A. Fessler, J.M. Balter, R.I. Berbeco, S. Nishioka, H. Shirato, "Inference of hysteretic respiratory tumor motion from external surrogates: a state augmentation approach," Physics in medicine and biology **53**, 2923-2936 (2008).

[17] Y. Suh, S. Dieterich, B. Cho, P.J. Keall, "An analysis of thoracic and abdominal tumour motion for stereotactic body radiotherapy patients," Physics in medicine and biology **53**, 3623-3640 (2008).

[18] J.A. Ng, J.T. Booth, R.T. O'Brien, E. Colvill, C.Y. Huang, P.R. Poulsen, P.J. Keall, "Quality assurance for the clinical implementation of kilovoltage intrafraction monitoring for prostate cancer VMAT," Medical physics **41**, 111712 (2014).

[19] N. Bhagat, N. Fidelman, J.C. Durack, J. Collins, R.L. Gordon, J.M. LaBerge, R.K. Kerlan, Jr., "Complications associated with the percutaneous insertion of fiducial markers in the thorax," Cardiovasc Intervent Radiol **33**, 1186-1191 (2010).

[20] D.P. Harley, W.S. Krimsky, S. Sarkar, D. Highfield, C. Aygun, B. Gurses, "Fiducial Marker Placement Using Endobronchial Ultrasound and Navigational Bronchoscopy for Stereotactic Radiosurgery: An Alternative Strategy," Ann Thorac Surg **89**, 368-373 (2010).

[21] H. Bahig, M.P. Campeau, T. Vu, R. Doucet, D. Beliveau Nadeau, B. Fortin, D. Roberge, L. Lambert, J.F. Carrier, E. Filion, "Predictive parameters of CyberKnife fiducial-less (XSight Lung) applicability for treatment of early non-small cell lung cancer: a single-center experience," International journal of radiation oncology, biology, physics **87**, 583-589 (2013).

[22] K. Yoon, J. Kwak, B. Cho, S. Song, S. Lee, S. Ahn, S. Nam, "Development of New 4D Phantom Model in Respiratory Gated Volumetric Modulated Arc Therapy for Lung SBRT," PROGRESS in MEDICAL PHYSICS **25**, 100-109 (2014).

[23] J. Yue, X. Sun, J. Cai, F.F. Yin, Y. Yin, J. Zhu, J. Lu, T. Liu, J. Yu, X. Shi, J. Song, "Lipiodol: a potential direct surrogate for cone-beam computed tomography image guidance in radiotherapy of liver tumor," International journal of radiation oncology, biology, physics **82**, 834-841 (2012).

[24] A. Nobah, S. Aldelaijan, S. Devic, N. Tomic, J. Seuntjens, M. Al-Shabanah, B. Moftah, "Radiochromic film based dosimetry of image-guidance procedures on different radiotherapy modalities," Journal of applied clinical medical physics / American College of Medical Physics **15**, 5006 (2014).